

Title: Simulations and observation of nonlinear internal waves on the continental shelf: Korteweg-de Vries and extended Korteweg-de

5 **Vries solutions**

First Author: Kieran O'Driscoll

Second Author: Murray Levine*

10 First Author address:

Kieran O'Driscoll

School of Natural & Built Environment

Queen's University Belfast

email: kieran.odriscoll@qub.ac.uk

15 Tel: +44 (0)28 9097 4204

Fax: +44 (0)28 9097 4278

*deceased

20

25

Simulations and observation of nonlinear internal waves on the continental shelf: Korteweg-de Vries and extended Korteweg-de Vries solutions

Kieran O'Driscoll¹, Murray Levine*

5 ¹Department of Civil Engineering, Queen's University Belfast, Belfast, BT9 1NN, Northern Ireland

*deceased

Correspondence to: Kieran O'Driscoll (kieran.odriscoll@qub.ac.uk)

Abstract. Numerical solutions of the Korteweg-de Vries (KdV) and extended Korteweg-de Vries (eKdV) equations are used to model the transformation of a sinusoidal internal tide as it propagates across the continental shelf. The ocean is idealized as being a two-layer fluid, justified by the fact that most of the oceanic internal wave signal is contained in the gravest mode. The model accounts for nonlinear and dispersive effects but neglects friction, rotation, and mean shear. The KdV model is run for a number of idealized stratifications and unique realistic topographies to study the role of the nonlinear and dispersive effects. In all model solutions the internal tide steepens forming a sharp front from which a packet of nonlinear solitary-like waves evolves. Comparisons between KdV and eKdV solutions is explored. The model results for realistic topography and stratification are compared with observations made at moorings off Massachusetts in the Middle Atlantic Bight. Some features of the observations compare well with the model. The leading face of the internal tide steepens to form a shock like front, while nonlinear high frequency waves evolve shortly after the appearance of the jump. Although not rank ordered, the wave of maximum amplitude is always close to the jump. Some features of the observations are not found in the model. Nonlinear waves can be very widely spaced and persist over a tidal period.

1. Introduction

Internal waves are present throughout earth's oceans wherever there is stratification, from the shallowest near-shore waters to the deepest seas. Internal waves are important to physical oceanographers because they transport momentum and energy, horizontally and vertically, through the ocean, e.g. Munk (1981), Gill (1982). They provide shear to turbulence which results in energy dissipation and vertical mixing, e.g. Holloway (1984), Sandstrom & Elliott (1984). Biological oceanographers are interested because the internal waves carry nutrients onto the continental shelf and into the euphotic zone, e.g. Shea & Broenkow (1988), Sandstrom & Elliott (1984), and Holloway et al. (1985). They are of interest to geological oceanographers because the waves produce sediment transport on the shelf, e.g. Cacchione & Drake (1986). Civil, hydraulic and ocean engineers are interested because the internal waves generate local tidal and residual currents, e.g. Willmott & Edwards (1987), which can cause scour on nearshore as well as offshore structures, e.g. Osborne et al. (1978). Large nonlinear IWs are also of interest to the navy because they cause large vertical displacements and large vertical velocities that may affect underwater operations.

This study is focused on the internal tide and subsequent evolution of nonlinear waves. Internal waves in the ocean span the frequency spectrum from the buoyancy frequency, N , to the inertial frequency, f . However, the internal, or baroclinic, tide accounts for a large fraction of the energy contained in these waves. The internal tide is generated by the interaction of barotropic tidal current with topography and not directly by the gravitational attraction of sun and moon. The properties and propagation of linear internal tide and waves have been treated in detail by many investigators, see, for example, Garrett & Munk (1979), or the monographs by Gill (1982), Lighthill (1978), or Apel (1987).

As the internal tide shoals, the nonlinear terms in the Navier-Stokes equations become important. These tidal waves of finite amplitude may evolve into packets of high frequency nonlinear waves. The equations describing these waves are much more complex than the linear equations and few mathematical solutions have been found.

5 We are interested in nonlinear internal waves because they are a very energetic part of the signal in time series that we have observed on continental shelves and in the shallow ocean. We are guided by numerical solutions of Korteweg-de Vries (KdV) type equations that incorporate both weak nonlinear and weak dispersive effects.

The state of the art on the evolution of internal solitary waves across the continental shelf is
10 reviewed in Grimshaw et al. (2010). Grimshaw et al. (2004) simulated the transformation of internal solitary waves across the North West shelf of Australia, the Malin shelf edge, the Arctic shelf; Holloway (1987) discussed the evolution of the internal tide in a two-layer ocean on the Australian North West Shelf. Our model simulations of the evolution of the internal tide across Middle Atlantic Bight topography are unique since these waves have never been modelled across such topography and stratifications, and
15 the model results are compared with observations made at moorings off Massachusetts during the Coastal Mixing and Optics (CMO) Experiment. For the model cases of linear bottom sloping realistic topography, whereas most studies have focused on the behaviour of a single soliton, this work is concerned with the development and evolution of a packet of solitary waves.

The goal of this paper is to study the observed variability in the evolution of the internal tide as it
20 crosses the continental shelf resulting from different stratifications and varying topography.

In section 2, the model framework is presented, and model runs and results of simulations are

discussed for cases of linearly sloping bottom topography and that at the site of the Coastal Mixing and Optics experiment (CMO). Model results are compared with data and observations collected at the CMO site in section 3. A summary and conclusions are presented in section 4.

5 2. Two-Layer Model

We are interested in modeling the evolution of the internal tide as it propagates shoreward from the shelf break. Since the greatest oceanic signal is the first internal mode, the stratification of the continental shelf/slope region is modeled as a two-layer fluid. This approximation greatly simplifies the problem; the numerical scheme is much less complex for the two-layer case than the continuously stratified case, and the results are easier to interpret. Using this model configuration, we study the propagation of the internal tide over linear sloping and CMO topography. All cases have been run within the quadratic nonlinear framework of the KdV equation, and the results are compared with an extended form of it, the eKdV model.

For the KdV Eq. (1) and eKdV Eq. (2) to be valid, the leading two terms must constitute the

$$15 \quad \eta_t + c\eta_x + \alpha\eta\eta_x + \beta\eta_{xxx} = 0 \quad 1$$

$$\eta_t + c\eta_x + (\alpha + \alpha_1\eta)\eta\eta_x + \beta\eta_{xxx} = 0 \quad 2$$

primary balance. The nonlinear and dispersive terms can become important, but the assumptions leading to the KdV and eKdV equations are violated if either of the nonlinearity or dispersion terms approach the magnitude of the leading terms. Nonlinear transformation of the internal tide leads to the generation of nonlinear waves which tend to become solitary-like in form as the dispersive term becomes important.

Note, the KdV equation is well known to be a suitable physical model for describing weakly nonlinear advective effects and linear dispersion in internal waves. It was originally developed by Benney (1966) and extended to second order by Lee & Beardsley (1974). The KdV Eq. (1) and eKdV Eq. (2) equations are derived following the procedure of Lee & Beardsley (1974) and the discussion by Lamb & Yan (1996). The two-layer KdV model approximation is discussed in Grimshaw et al. (2002), and justified since most of the energy in the ocean appears to be contained in the first mode anyway, see e.g. Alford & Zhao (2007). The coefficients of the KdV and eKdV equations are greatly simplified for a two-layer fluid, e.g. Ostrovsky & Stepanyants (1989). The problem has been investigated for slowly varying topography and stratification by Grimshaw (1979) and Pelinovsky et al. (1977). An interesting reference is Lamb & Xiao (2014), who took a similar approach to ours, comparing predictions of the KdV and eKdV models, and also the RLW equation, with fully-nonlinear numerical simulations for two-layer stratification over selected topographies. See O’Driscoll (1999) for a full discussion of our experiments.

For all simulations the density difference between the two layers is chosen to be a constant: $g\Delta\rho/\rho = .014 \text{ m/s}^2$, a representative value for the Coastal Mixing and Optics (CMO) experiment (Levine & Boyd, 1999), for example at a mooring in the Middle Atlantic Bight located at 40.5°N, 70.5°W, and also in agreement with the stratification near the mooring location displayed in Barth et al. (1998).

2.1 The Korteweg de Vries (KdV) Model solutions

Using the KdV equation, we investigate 2 cases with constant sloping bottom, horizontal and sloping interface, and finally make model runs with realistic topography at the CMO site.

For convenience in solving the equation, we avail of a transformation, utilized by Pelinovsky & Shavratsky (1976), of the space and time variables x and t to variables l and s , respectively, given by

$$s = \int_0^x \frac{dx}{c(x)} - t, \quad l = x. \quad 3$$

The transformed eKdV is then

$$5 \quad \zeta_l + \frac{1}{c^2 \sqrt{Q}} (\alpha + \alpha_1 \zeta) \zeta \zeta_s + \frac{\beta}{c^4} \zeta_{sss} = 0 \quad 4$$

where $\zeta = \eta \sqrt{Q(l)}$, $Q = \frac{Mc^3}{M_0 c_0^3}$, $M = \frac{h_1 + h_2}{h_1 h_2}$, and 0 subscripts represent initial values. The

transformation scales time so that disturbances traveling at the linear speed, c , remain at constant s . The system is often referred to as a slowness coordinate system. Because ζ varies relatively slowly in l/c

compared to s , terms such as $c\zeta_l$ are neglected relative to ζ_s . The transformed KdV equation is the

10 same as the transformed eKdV equation with $\alpha_1 = 0$. See O'Driscoll (1999) for further details.

2.1.1 Constant Bottom Slope

The propagation of the internal tide along constant sloping topography was studied for cases of constant upper layer thickness (Case A) and sloping interface (Case B), both of which are possible on
15 continental shelves. We chose starting layer thickness at $l = 0$ $h_1 = 50m$ and $h_2 = 150m$, with bottom slope of $1/1000$ so that total depth decreases from 200 to $0 m$ over a distance of $200 km$.

We first investigate the case of constant sloping bottom with constant upper layer thickness (Case A). The value of c decreases in shallow water, while $\alpha \rightarrow 0$ as $h_2 \rightarrow h_1$ at water depth of $100 m$ (Fig. 1a).

Seaward of this depth where $h_2 > h_1$, $\alpha < 0$ and solitary waves are waves of depression, whereas shoreward of this depth ($h_2 < h_1$), $\alpha > 0$ and solitary waves exist as waves of elevation only. $\beta \rightarrow 0$ as the product $h_2 h_1 \rightarrow 0$. As the magnitude of α is initially relatively large we expect the sinusoidal internal tide to transform rapidly resulting in the formation of several nonlinear waves. Since $\alpha \rightarrow 0$, these waves
5 may not be so nonlinear as to violate the weakly nonlinear constraint on the KdV model. However, because the value of α rapidly increases for $l > 100\text{km}$, we expect the waves of elevation to become highly nonlinear thereby possibly violating the weakly nonlinear condition.

Figs. 1b and c show the internal tide signal for Case A at different values of l and also at different water depths. The internal tide steepens and rapidly becomes nonlinear, resulting in the generation of a
10 shock-like front and subsequent undulations by $l \approx 50\text{km}$. Shoaling further, the internal tide becomes more nonlinear with the oscillations starting to resemble solitary waves by $l = 70\text{km}$. However, the waves never develop into mature internal solitary waves since the magnitude of α continually decreases. By $l = 90\text{ km}$ the waves resemble a symmetric, dispersive packet, as further evidenced by Fig. 2a. Initially the relatively large magnitude of α resulted in the rapid steepening of the internal tide. However, as the value
15 of $\alpha \rightarrow 0$ the nonlinear waves are prevented from developing into solitary waves, since higher order terms (neglected in KdV) become of order α or larger and thus cannot be ignored, thereby rendering the KdV model invalid in this neighborhood. At $l = 100\text{km}$ the packet certainly looks symmetrical about a horizontal axis, that is to say the waves are neither polarized as waves of depression nor elevation, since KdV solitary waves cannot exist when $\alpha = 0$. At 115km the waves have switched polarity; they have
20 become waves of elevation, a result of α having become positive. This transition is seen in Fig.2b where

the leading waves are compared with sech^2 solitary form. Beyond 100km the waves rapidly approach solitary waves of elevation since α becomes large quickly.

As the internal tide propagates into shallow water the leading face of the wave steepens but the decreasing magnitude of α causes this steepening to slow down and there is virtually no change in wave slope steepness between 70 and 90 km . The rate of change of the slope of the leading face changes sign when α becomes positive and the slope steepens rapidly, while the back face of the internal tide slackens. The steepening of the leading wave will lead to the formation of a second shock-like front (or a “reverse hydraulic jump” as has been described by Holloway et al., 1997). Fig. 1c gives a clear picture of the wave speed: the leading solitary-type wave initially travels with speed very slightly greater than c but becomes slower than c when $l \sim 90\text{km}$. The second solitary-type wave also has initial speed greater than c but becomes slower than c at $l \sim 80\text{km}$. All of the other waves travel with phase speed less than c . For $l > 100\text{km}$ all waves travel with speed less than c , the reason becomes clear upon examination of Fig. 2a which plots the difference between the magnitudes of the nonlinear and dispersive terms.

The leading waves are slightly more nonlinear than dispersive when $l \approx 70\text{ km}$ but become less so as l approaches 100 km . When $\alpha = 0$ ($l = 100\text{km}$) the value of the nonlinear term is zero and the waves look like a dispersive packet. Since $\alpha > 0$ for $l > 100\text{ km}$, the nonlinear term is again a factor and the waves become a hybrid by $l = 115\text{km}$, interchanging back and forth across the length of the wave between being more nonlinear and dispersive. The waves travel slower than c since the magnitude of the dispersive term is slightly greater than the nonlinear term.

For Case B with constant sloping bottom and sloping upper layer, we also begin in 200m water with $h_1 = 50\text{m}$, $h_2 = 150\text{m}$. In this instance the bottom slope is again $1/1000$ and the interface slope is

1/4000 such that both layers vanish simultaneously at $l = 200 \text{ km}$. KdV parameter values are shown in Fig. 3a. The magnitude of α increases from $l = 0$ all the way to the shallowest water, unlike Case A where α passes through zero, so we expect the internal tide to become nonlinear sooner than for Case A, and any solitary waves to remain as waves of depression. We do, however, expect the waves to become physically unstable, leading to a Kelvin-Helmholtz instability (see e.g. Cushman-Roisin & Beckers 2011), a result of the increasing magnitude of the nonlinear parameter combined with the decreasing value of the dispersive parameter. This combination of events will result in the weakly nonlinear, dispersive KdV becoming invalid at $l = 95 \text{ km}$. Fig. 3b is a plot of the internal tide for Case B at several values of l . The internal tide steepens rapidly and a shock-like wave, followed by undulations, has evolved from the transforming tide by $l = 40 \text{ km}$. The internal tide continues to steepen and several nonlinear waves have formed by $l = 55 \text{ km}$. These leading nonlinear waves mature into rank ordered solitary waves by 65 km . Fig. 3c shows that most of the solitary waves eventually travel with phase speed greater than c . The waves are more nonlinear than dispersive and the increasing value of the nonlinear parameter combined with the diminishing value of the dispersive parameter leads to the model becoming numerically unstable (O'Driscoll 1999).

2.1.2 Realistic topography and stratification

The CMO site was located in the Middle Atlantic Bight. CTD profiles were made across the continental shelf from shallow water to beyond the continental slope. Boyd et al. (1997) have concluded that the internal tide at the site is primarily a first mode internal wave, further justifying our choice of a

two-layer model. An upper layer thickness of 25 m is a representative average value for the duration of the experiment (July and August 1996).

Fig. 4a shows KdV parameter values as a function of l . Though undulating, the bottom topography is similar to the constant sloping bottom cases. Recall that we chose an upper layer depth of 50 m for Case A, whereas here we have chosen $h_1 = 25$ m. α starts out negative with relatively large magnitude. The magnitude decreases, similar to Case A, changing sign as the bottom shoals and $h_1 > h_2$ when the value increases rapidly. Values of β , c and the horizontal variability parameter, Q , are similar to Case A. Figs. 4b and c show results for tidal forcing of amplitude 2 m at 180 m water depth. The internal tide evolves similarly to Case A. A shock-like front has formed on the back-face of the internal tide at $l = 40$ km. Several nonlinear waves have formed by $l = 60$ km (mooring location) with the leading 4 – 5 waves appearing like solitary waves of depression and the trailing waves looking more like a dispersive packet. Several more waves have formed by 80 km but the number of solitary-like waves seems to have been reduced to the leading two waves. All of the trailing waves do appear as a dispersive packet since the magnitude of α has decreased. More waves continue to form but by 100 km the packet is neither a pack of waves of elevation nor depression, not unlike Case A. Beyond $l = 125$ km, α becomes large, the waves reverse polarity and rapidly develop into mature solitary waves of elevation. The results show that the CMO case and Case A are similar, though more solitary waves have formed for the CMO case, due to the fact that at the CMO site the value of α is initially twice that of Case A. The internal tide becomes unstable beyond $l = 130$ km, a result of the increasing value of the nonlinearity parameter combined with the vanishing dispersion parameter. Fig. 4c is a plot of the evolution of the internal tide as it propagates over the continental shelf, increasing in l . The leading solitary-like waves initially travel with speed very

slightly greater than c , as in Case A. The waves slow down to travel at speed c where $l \approx 90 \text{ km}$ and α is very small. Wave speed then becomes slightly slower than c but faster and more complicated than Case A, due to the undulating topography.

The difference in magnitudes of the nonlinear and dispersive terms, $\chi = \left| \frac{\alpha}{c^2} \eta \eta_s \right| - \left| \frac{\beta}{c^4} \eta_{sss} \right|$, is

5 plotted in Fig. 5. The leading 2-3 three waves are initially more nonlinear than dispersive but the diminishing magnitude of α leads to the waves becoming more dispersive-like and the waves begin to slow down. The negligible value of α between $l = 100 - 115 \text{ km}$ results in the waves acting very much like a dispersive packet and they travel with wave speed slightly less than c . The increasing value of α after it passes through zero, leads to the nonlinear term becoming almost the same order of magnitude as
 10 the dispersive term before the model becomes numerically unstable shortly beyond $l = 130 \text{ km}$.

2.2 The extended Korteweg - de Vries (eKdV) model

The model runs discussed in section 2.1 were also made with the eKdV equation. The ratio of the nonlinear parameters, $\frac{\alpha}{\alpha_1} = 4 \frac{h_1 - h_2}{h_1 h_2 (h_1^2 + h_2^2 + 6h_1 h_2)}$ (see e.g. Ostrovsky & Stepanyants, 1989) is the
 15 theoretical maximum amplitude for the solitary wave solution to the eKdV equation. The ratio of the quadratic to cubic nonlinear terms in this equation depends upon displacement height, η , and is given by
 $\frac{\alpha}{\alpha_1 \eta}$.

For Case A the ratio $\frac{\alpha}{\alpha_1}$ passes through zero ($h_1 = h_2$) and we expect the cubic nonlinear term to be important. The results of this model run are shown in Fig. 6. The internal tide evolves similar to the

KdV case (Fig. 1b) with a shock-type wave followed by several nonlinear oscillations on the back face of the internal tide at $l = 50km$. The internal tide in both frameworks look similar at $70 km$ where several nonlinear waves of depression have been formed. The KdV solitary-like waves flip polarity at $100 km$ due solely to the fact that α changes sign there.

5 For the CMO case, comparison of KdV and eKdV results shows a more significant difference than for Case A. Fig. 7a-c show the KdV and eKdV model results for a $4m$ internal tide having propagated $60 km$ to a water depth of $69 m$. The leading KdV model solitary wave (solid line) arrives at the CMO central mooring ~ 0.1 tidal period ahead of the leading eKdV model solitary wave (broken line). The KdV and eKdV models are so different at the CMO site when compared to Case A because the magnitude of α_1 is

10 greater at the CMO site. Though the magnitude of α is less in Case A, the fact that the magnitude of α_l is so small when compared to α means the addition of the cubic nonlinear term does little to change the KdV results. This is not true at the CMO site where the greater magnitude of α_l is the reason for the difference between the KdV and eKdV frameworks, particularly as the internal tide propagates into shallower water and the magnitude of the ratio $\frac{\alpha}{\alpha_1}$ is much greater for Case A, where h_1 and h_2 are,

15 respectively, twice and less than that at the CMO site. Comparing the leading waves from the eKdV and KdV solutions reveals a fundamental difference in wave form; the KdV waves are taller and thinner (Fig. 7c). Solitary type solutions to the KdV (sech^2) and to the eKdV (\tanh , also known as ‘table-top’ waves) are fitted to the leading waves (Fig. 7d-e). The leading wave in the KdV model is very well approximated by a sech^2 wave. The lead wave in the eKdV model is neither well approximated by sech^2 or table-top

20 wave, but appears to be a hybrid between the two. Fits of sech^2 and table-top waves were made by subjectively choosing values of η_0 and v , respectively, while using the value of KdV and eKdV

parameters for 69m water depth. Note that the amplitude of the table-top wave is limited to $\frac{\alpha}{\alpha_1}$. Increasing

ν only serves to make the waves wider once its value is close to one (see e.g. O’Driscoll 1999). Amplitude and width of the leading waves in the packet are also compared in Fig. 8a. The width is defined as the time it takes the wave to pass a fixed point, as measured at 42% of the amplitude. Results from a range of different tidal amplitudes are also shown. For reference, the dotted lines represent sech^2 and table-top waves for the local values of parameters h_1 , h_2 , and $g\Delta\rho/\rho$. For KdV the leading wave of the 2m tide always has amplitude greater than the second and the amplitudes of subsequent waves decrease in a rank ordered fashion. The leading wave is slightly thicker than the trailing ones which are all approximately equal in width. For the eKdV the leading wave has larger amplitude and is thicker than the trailing waves. For the KdV model with 4m amplitude tide all the waves fall on the same spot on the sech^2 curve. For the eKdV model with 4m amplitude tide, the waves appear on the ‘thick’ side of the sech^2 curve with the lead wave the most removed from the KdV theoretical curve. The same is true for amplitudes of 5m and 6m. The eKdV model waves appear to be evolving toward the theoretical eKdV ‘tanh’ curve. Note that the amplitude of many of these waves exceed the maximum amplitude of table-top/tanh waves of 9 m as determined by the local parameters at the CMO site.

To learn more about the evolution of a sine wave to waves with sech^2 and table-top form, we ran the model with constant parameters (flat bottom) using values at the mooring site. The runs were made with initial tidal amplitudes of 1, 2 and 4 m in both KdV and eKdV frameworks and the width vs. amplitude for the first and second wave in each packet is plotted at various increments of l (Fig. 8b). The KdV waves grow in amplitude with approximately constant width before turning to hug the theoretical

KdV line. They then decrease in amplitude while increasing slightly in thickness. Though the KdV model waves continue to evolve, most of them can be well approximated as being ‘sech²’ waves after $\sim 100km$. For the eKdV case, the waves are initially close to the theoretical sech² KdV curve. The waves move slowly towards the theoretical eKdV tanh curve, ultimately decreasing in amplitude and increasing in thickness. The last points have been plotted after the internal tide has propagated $\sim 240km$. It appears that these waves are evolving toward table-top form, but mature over a relatively long distance. Also, the amplitudes of the waves are greater than the theoretical eKdV maximum but their magnitudes decrease as the tide evolves.

Another investigation to explore the evolution in the eKdV model (constant parameters) was made using an initial condition of a sech² wave, the solitary wave solution to the KdV equation. sech² amplitudes of 4m, 7m, 9m, and 13m (Fig. 8c) were chosen. The sech² waves are rapidly transformed to table-top waves, e.g. the 4 examples plotted reach the theoretical eKdV curve after the wave has propagated about 10 km. A solitary sech² wave evolves much more rapidly to table-top form (Fig. 8c), as opposed to when it is part of a packet of waves (Fig. 8b). The reason for this has not been thoroughly investigated, but provides caution for treating a packet as a group of non-interacting waves.

3. Observations of Nonlinear Internal Waves

The data to be presented and discussed was collected during the CMO, for location see Fig. 9. The CMO experimental field program was conducted to increase our understanding of the role of vertical mixing processes in determining the mid-shelf vertical structure of hydrographic and optical properties. The field program was conducted on a wide shelf so as to reduce the influences of shelf break and nearshore

processes. The data we discuss was collected from the CMO Central Mooring in July and August 1996, a time when a strong thermocline is present as a result of large-scale surface heating, Boyd et al. (1997).

3.1 Observations during the Coastal Mixing and Optics Experiment

5 The Central Mooring of the CMO experiment was located at $40^{\circ} 29.50' \text{ N } 70^{\circ} 30.46' \text{ W}$ in water depth of 69 m. A total of 24 temperature recorders and 5 conductivity sensors were distributed along the mooring. Currents were measured at 14 depths from an ADCP placed a few metres above the bottom.

 Boyd et al. (1997) have calculated the first mode internal wave amplitude from the velocity time series for the period 29 July to the 31 August 1996 (year day 210 - 245, Fig. 10 i)). The dominant
10 barotropic tidal signal in the Middle Atlantic Bight is semi-diurnal, and is strongest over the period day 241-245 during spring tide (Fig. 11). A semi-diurnal signal is apparent in the first mode record, particularly during the spring tide period. A spectrum of the first mode amplitude (Fig. 12) shows energy peak at both low and high tidal frequencies. Much of the high frequency energy is due to bursts or pulses of high frequency nonlinear internal waves that occur for a short period during the semi-diurnal tidal
15 cycle. These nonlinear internal waves propagate shoreward across the continental shelf to the south of Martha's Vineyard. The energy at high frequency is greater over the period day 241-245 during spring tides (Fig. 12). There is a clear maximum in energy at 2 cpd over this period, and a significant amount of energy is also contained at 4 cpd. The energy rapidly drops for frequencies greater than 4 cpd but there is a significant increase in energy at $\sim 50 \text{ cpd}$ and $\sim 90 \text{ cpd}$. To help interpret these observations, we
20 compare them with the two-layer eKdV model using the CMO parameters. Since we do not know where the internal tide is generated or its amplitude, the model was run assuming a sinusoidal internal tide at

distances of 24 km, 48 km and 60 km seaward of the mooring site. Three initial amplitudes of 2 m, 4 m and 6 m were used at each distance. Fig. 10 iii) shows the internal tide as it appears at the CMO mooring site for these nine cases. In all instances, the leading face of the periodic sinusoidal wave slackens (or flattens) as the internal tide propagates shoreward. This is followed by a steepening of the back face which
5 develops into a shock-like front. The shock-like front is followed by oscillations which subsequently evolve into a packet of solitary-like waves.

This same pattern can often be seen in the observed time series of the first internal mode. Fig. 13 shows several individual jumps at the CMO mooring. Fig. 13 i) (top left panel) shows first modes which best match the model results of Fig.10 iii). Some features of the observations compare well with the
10 model. The slackened leading face of the tide is always followed by a steep - almost shock like - front followed by several highly nonlinear short period waves. Although not rank ordered, the largest amplitude wave in the observed packet is always at or near the jump. The model results show that the amplitude of the jump is greater for larger initial condition, and decreases with distance from the point of generation. Although nonlinear waves continue to evolve, their amplitudes decrease as they propagate shoreward
15 from their generation point, and they become 'thicker', i.e. they become more table-top like. Though the modelled waves have amplitudes less than the theoretical tanh limit for local eKdV parameters, they nonetheless fit the shape of several observed waves at the CMO site.

There are also features of the observations that are not found in the model. Fig. 13 i) top left (f) and (g) differ in that the packet that follows the shock-like front, persists until the end of the tidal period, and the waves are spread apart from each other. Fig. 13 i) top left (c) shows two packets of solitary-like
20 waves propagating past the mooring site over a tidal period. The leading slackened face is followed by a

shock-like front and a packet of solitary waves. The trailing face then slackens to assume a slope similar to the leading face but a second shock-like front, followed by a packet of solitary waves, passes before the end of the tidal period. This could be from a second internal tide front coming from another generation site, there can be overlapping semi-circles of internal wave fronts from multiple generation sites, see for
5 example discussion in Apel et al. (1988). Another possible generation mechanism is the nonlinear evolution of inertia-gravity waves forming behind internal solitary waves due to rotation, see further in Grimshaw et al. (2014) and Lamb & Warn-Varnas (2015). It is also possible that multiple packets form each tidal period, due to different generation mechanisms such as multiple tidal constituents or harmonics of a tidal components as found, for example, at the site of the Littoral Optics Experiment where the 4th
10 harmonic of the semi-diurnal tide was used to successfully simulate the evolution of the internal tide (O'Driscoll 1999).

Another common observation that is not found in the model results is a ‘drop’ in amplitude before the jump that occurs at the beginning of the wave packet. Fig. 13 top left (h) shows that the first
15 internal mode drops between day 243.5 and 243.6 but the slackening slope is restored before the arrival of the jump and packet of solitary waves. Similar ‘drops’ also occur in Fig. 13 top left (b) and (e) and top right (a) and (i). Another phenomenon observed is that the slope of the leading face of the tide changes sign before the packet in several of the examples in Fig. 13 top right. In Fig. 13 top right (h) the low frequency slope changes sign at day 236, and the solitary waves appear as usual ahead of the
20 trailing, low frequency signal. The signal becomes even more complicated when both a ‘drop’ and low frequency slope change are present, e.g. Fig. 13 top right (d). In this case, the slope of the leading

slackening low frequency signal changes sign at day 242.5 and is followed by a packet of four solitary waves. The low frequency signal is restored before the passage of a jump followed by a packet of five large solitary waves. The trailing face retains the slope of the low frequency signal. Fig. 13 bottom shows a series of jumps which are more complex than those in the top panels, though they retain the
5 basic structure of the model results over the tidal period.

To examine the details of the wave packets themselves, the width vs. amplitude was estimated for each wave from all events during the period day 210-245 (Fig. 14). These waves are plotted along with the leading two waves from six of the nine model runs shown in Fig. 10 iii). Also shown are the theoretical relations for solitary waves for the eKdV and KdV equations using CMO site parameters. The observed
10 nonlinear waves vary greatly in amplitude and width, generally having amplitudes of 5 – 25 metres, and widths of 200 – 600 seconds. Larger amplitude observed waves are well approximated by model runs with large initial amplitude, particularly the 4m model. The 6m model run from 24km seaward of the CMO site is also a very good match for several of the observed waves. A large fraction of observed waves with amplitude less than 15m, and particularly less than 10m, are much ‘thinner’ than model waves with
15 similar amplitudes. However, it seems reasonable to say that the observed waves are a good fit to the model waves.

While some features of the observations are reproduced in the model, there are many differences. The eKdV model used here is highly idealized. There are many effects that have not been considered, including bottom and internal friction, earth’s rotation and mean shear. Given these
20 limitations, we conclude that the observations are reasonably well matched by our model.

4. Summary and conclusions

Observations of highly nonlinear internal waves contained in the first mode time series on the mid-continental shelf and in current meter records in shallow water have led us to investigate the transformation of the shoaling internal tide. Observations were made in the mid-continental shelf at the site of the Coastal Mixing and Optics Experiment (CMO). An existing model based on generalized KdV and eKdV equations has been simplified for use in a two-layer ocean, which is representative of realistic stratification. The model accounts for weakly nonlinear and dispersive properties of the internal tide. Earth's rotation, internal dissipation, bottom friction, and internal shear are not included. The internal tide was forced with a periodic sinusoidal boundary condition and allowed to propagate shoreward.

The model was first run within a KdV framework with realistic continental shelf, constant sloping bottom with flat and sloping interface, and CMO shelf parameters. The internal tide steepens on its back face as it propagates shoreward, a direct result of the much greater magnitude of the nonlinear term in comparison with the dispersive term. Nonlinear waves evolve from the internal tide after the back face forms a shock-like front. The waves can appear as a rank ordered packet with the leading waves traveling fastest, since they are the most nonlinear. The leading waves of depression usually travel faster than the linear wave speed, c , and nearly fit solitary wave form for local KdV parameters ("sech²"). Waves of elevation also develop into sech² waves.

The model runs made within the KdV framework were also made within the eKdV framework which includes a cubic nonlinearity term scaled by α_1 . The results may or may not be similar, depending upon the ratio of the two nonlinear terms, $\frac{\alpha}{\alpha_1 \eta}$. If this ratio is large (much greater than one) the cubic nonlinear term is not important and the KdV and eKdV results are similar. If the ratio is of order one or less the

eKdV may evolve differently from the KdV. For the constant bottom slope simulations the model results were similar in both frameworks. However, there are some significant differences to the waves that cross the shelf using CMO parameters. The modeled leading waves at the CMO mooring site were much ‘thicker’ than sech^2 waves with local KdV parameters, but they had not quite developed into solitary wave solutions of the eKdV equation (‘tanh’ or table-top waves).

To better understand the evolution of waves toward table-top form in an eKdV framework, without the complications of varying parameters, model runs were made using constant eKdV parameters representative of the CMO site. Upon formation, the leading waves of the packet are similar to sech^2 waves. The waves become ‘thicker’ and tend toward the table-top form upon further propagation, but never reach the theoretical tanh curve in our limited domain. To help understand why the evolution of waves from being close to sech^2 waves to being close to tanh waves was so slow, the internal tide was forced with a sech^2 wave. The evolving sech^2 rapidly moves to the theoretical tanh curve for all amplitudes. We conclude that the interaction between the solitary like-waves in a packet slows them from evolving into exact solitary ‘ sech^2 ’ or ‘tanh’ waves.

Model runs with varying initial amplitudes and generation regions were made to help interpret the observations made at the CMO site. Some features of the observations compare well with the model. The leading face of the internal tide steepens to form a shock like front. Nonlinear high frequency waves evolve shortly after the appearance of the jump. Although not rank ordered, the wave of maximum amplitude is always close to the jump. Some features of the observations are not found in the model. Nonlinear waves can be very widely spaced and persist over a tidal period. The amplitude of the observed waves often decreases before the arrival of the jump, while the leading face may change slope before the jump arrives.

Individual observed waves were examined and the details compared to model results. The observed nonlinear waves vary greatly in amplitude and width, generally having amplitudes of between 5 and 25 metres, and widths of between 200 and 600 seconds. Larger amplitude waves are well approximated by waves evolving from large amplitude model waves. A large fraction of smaller amplitude observed waves, particularly less than 10 m, are thinner than model waves of similar amplitude. We conclude that the observed waves are a good match to modeled waves given the highly idealized eKdV model used, and the fact that we have neglected friction, rotation and mean shear.

Author Contribution

10 Kieran O'Driscoll conducted this work out while a graduate student at the College of Oceanic & Atmospheric Sciences, Oregon State University, in partial fulfillment of the degree of Master of Science. Murray Levine was the student's advisor.

Acknowledgements

15 Kieran O'Driscoll would like to thank Jack Barth for a considerable review of a previous version of this manuscript, and two referees for considerable reviews and helpful comments. This work was supported by funding from the Office of Naval Research and Oregon State University.

Competing interests: Kieran O'Driscoll declares that he has no conflict of interest.

20

25

References

- Alford, M.H. and Zhao, Z.: Global patterns of low-mode internal-wave propagation. Part I: Energy and energy flux. *J. Phys. Oc.*, 37, 1829-1848, 2007.
- Apel, J.R.: Principles of ocean physics, International Geophysics Series, Volume 38, Academic Press, pp. 5 634, 1987.
- Apel J.R., R.F. Gasparovic, D.R. and Thompson, B.L. Gotwols.: Signatures of surface wave/internal wave interactions: Experiment and theory." *Dyns. Atms. Ocs.*, 12, 89-106, 1988.
- Barth, J. A., Bogucki, D., Pierce, S. D., and Kosro, P. M.: Secondary circulation associated with a shelfbreak front. *Geophys.l Res. Letts.*, 25, 2761-2764, 1988.
- 10 Benney, D.J.: Long nonlinear waves in fluid flows. *J. Math. Phys.*, 45, 52 – 63, 1966.
- Boyd, T., Levine, M.D., and Gard, S.R.: Mooring observations from the Mid-Atlantic Bight, Oregon State University, Data Report 97-2, pp. 226, 1997.
- Cacchione, D.A. and Drake, D.A.: Nepheloid layers and internal waves over continental shelves and slopes, *Geo-Marine Lett.*, 6, 147-152, 1986.
- 15 Cushman-Roisin, B. and Beckers, J-M.: Introduction to geophysical fluid dynamics: physical and numerical aspects. Vol. 101. Academic Press, 2011.
- Garrett, C. and Munk, W.: Internal waves in the ocean, *Ann. Rev. Fluid Mech.*, 11, 339-369, 1979.
- Gill, A.E.: *Atmosphere-Ocean Dynamics*, Academic Press, Inc., pp.662, 1982.
- Grimshaw, R.: Slowly varying solitary waves. I. Korteweg - de Vries equation. *Proc. R. Soc., Lond., Ser.* 20 *A*, 368, 359-375, 1979.
- Grimshaw, R., Pelinovsky, D., Pelinovsky, E., and Slunyaev, A.: Generation of large-amplitude solitons in the extended Korteweg–de Vries equation. *Chaos: An Interdisciplinary Journal of Nonlinear Science*, 12, 1070-1076, 2002.
- Grimshaw, R., Pelinovsky, E., Talipova, T., and Kurkin, A.: Simulation of the transformation of internal 25 solitary waves on oceanic shelves. *J. Phys. Oc.*, 34, 2774-2791, 2004.
- Grimshaw, R., Pelinovsky, E., Talipova, T., and Kurkina, O.: Internal solitary waves: propagation, deformation and disintegration, *Nonlinear Processes in Geophysics*, 17, 633-649, 2010.

- Grimshaw, R., Guo, C., Helfrich, K. and Vlasenko, V.: Combined effect of rotation and topography on shoaling oceanic internal solitary waves, *J. Phys. Oc.*, 44, 1116-1132, 2014.
- Holloway, P.E.: On the semidiurnal internal tide at a shelf-break region on the Australian North-West Shelf, *J. Phys. Oc.*, 14, 1787-1799, 1984.
- 5 Holloway, P.E.: Internal hydraulic jumps and solitons at a shelf break region on the Australian North West Shelf. *J. Geophys. Res. Oc.*, 92, 5405-5416, 1987.
- Holloway, P.E., Humphries, S.E., Atkinson, M., and Imberger, J.: Mechanisms for nitrogen supply to the Australian North-West Shelf. *Aust. J. Mar. Freshw. Res.*, 36, 753-764, 1985.
- Holloway, P.E., Pelinovsky, E., Talipova, T., and Barnes, B.: A nonlinear model of internal tide
10 transformation on the Australian North West Shelf. *J. Phys. Oc.*, 27, 871-896, 1997.
- Lamb, K.G. and Yan, L.: The evolution of internal wave undular bores: Comparisons of a fully nonlinear numerical model with weakly-nonlinear theory, *J. Phys. Oc.*, 26, 2712 – 2734, 1996.
- Lamb, K. G. and Warn-Varnas, A.: Two-dimensional numerical simulations of shoaling internal solitary waves at the ASIAEX site in the South China Sea, *Nonlinear Processes in Geophysics*, 22, 289-312, 2015.
- 15 Lamb, K.G. and Xiao, W.: Internal solitary waves shoaling onto a shelf: Comparisons of weakly-nonlinear and fully nonlinear models for hyperbolic-tangent stratifications, *Ocean Model*, 78, 17-34, 2014.
- Lee, C. and Beardsley, R.C.: The generation of long nonlinear internal waves in a weakly stratified shear flow, *J. Geophys. Res.*, 79, 453-462, 1974.
- Levine, M. and Boyd, T.: Nonlinear internal wave observations on the continental shelf. In *The 1998
20 WHOI/IOS/ONR Internal Solitary Wave Workshop: Contributed Papers*, 1999.
- Lighthill, J.: *Waves in fluids*, Cambridge University Press, pp. 504, 1978.
- Munk, W.H.: Internal waves and small-scale processes. *Evolution of Physical Oceanography* (B.A. Warren & C. Wunsch, eds.), Chapter 9. MIT press, Cambridge Massachusetts, 1981.
- O’Driscoll, K.T.A.: Nonlinear internal waves on the continental shelf. MS Thesis, College Oceanic and
25 Atmospheric Sciences, Oregon State Univ., pp.125, 1999.
- Osborne, A.R., Burch, T.L., and Scarlet, R.I.: The influence of internal waves on deep-water drilling. *J. Pet. Technol.*, 30, 1497, 1978.

Ostrovsky, L. A. and Stepanyants, Y.A.: Do internal solitons exist in the ocean? *Rev. Geophys.*, 27, 293-310, 1989.

Pelinovsky, E. and Shavratsky, S. Propagation of nonlinear internal waves in the inhomogeneous ocean, *Izv. Atmos. Oceanic. Phys.*, 12, 41 – 44, 1976.

5 Pelinovsky, E., Shavratsky, S., and Raevsky, M.A.: The Korteweg de Vries equation for nonstationary internal waves in an inhomogeneous ocean, *Izv. Atmos. Oceanic. Phys.*, 13, 373 – 276, 1977.

Sandstrom, H. and Elliott, J.A.: Internal tide and solitons on the Scotian shelf: a nutrient pump at work., *J. Geophys. Res.*, 89, 6415-6426, 1984.

10 Shea, R.E., and Broenkow, W.W.: The role of internal tides in the nutrient enrichment of Monterey Bay, California, *Estuarine, Coastal and Shelf Sci.*, 15, 57-66, 1982.

Willmott, A. and Edwards, P.D.: A numerical model for the generation of tidally forced nonlinear internal waves over topography, *Cont. Shelf Res.*, 7, 457-484, 1987.

15

20

25

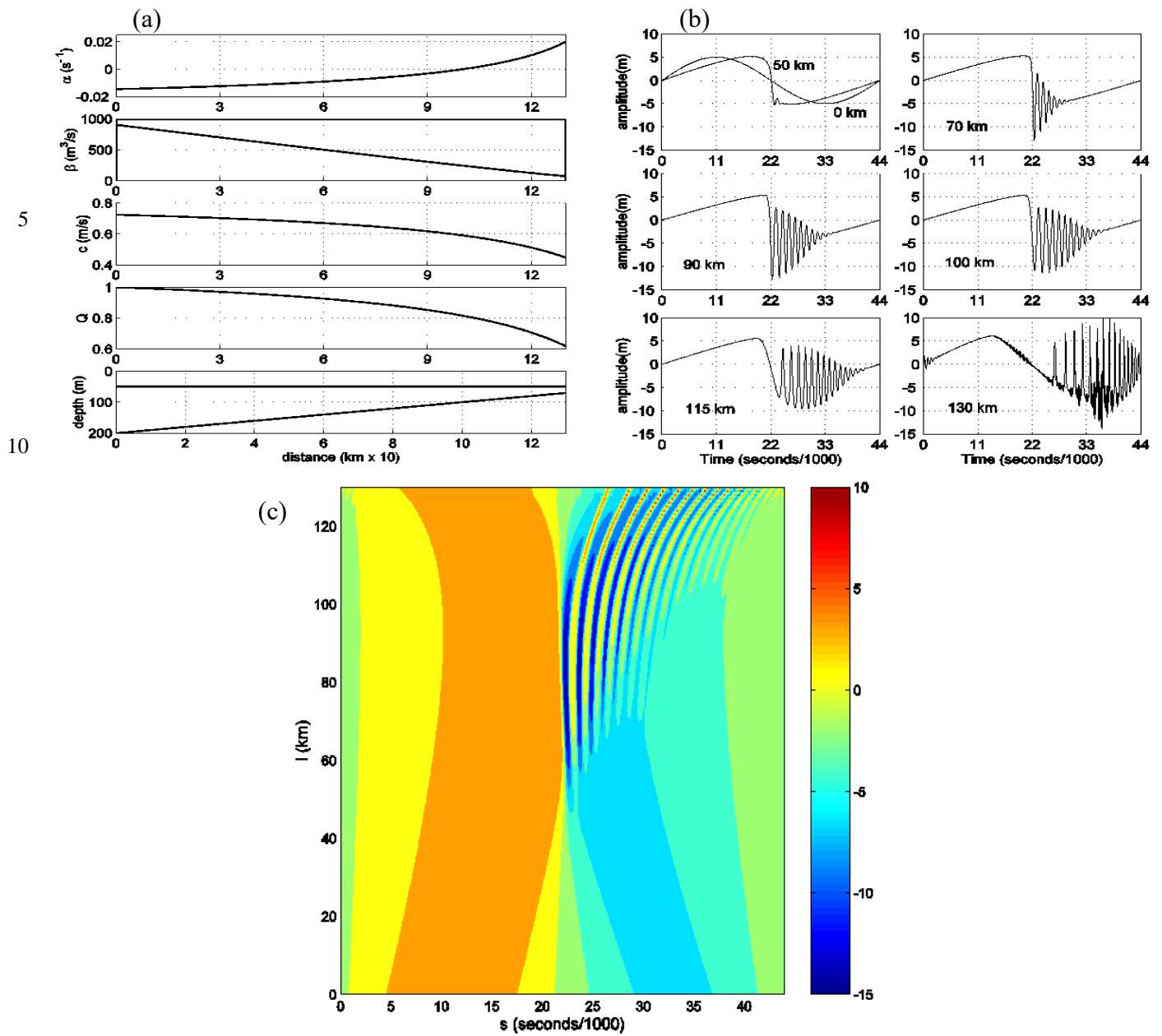


Fig. 1. Case A (constant sloping bottom with level interface, $h_l = 50$ m). KdV parameter values for quadratic nonlinear parameter, α , dispersion parameter, β , linear phase speed, c , horizontal variability factor, Q , and depth (a). Amplitude of the internal mode for two-layer fluid (b) at various distances from the boundary within KdV model framework and (c) as a function of distance l and time s within KdV model framework. The legend on the right corresponds to the amplitude of the waves (m).

15

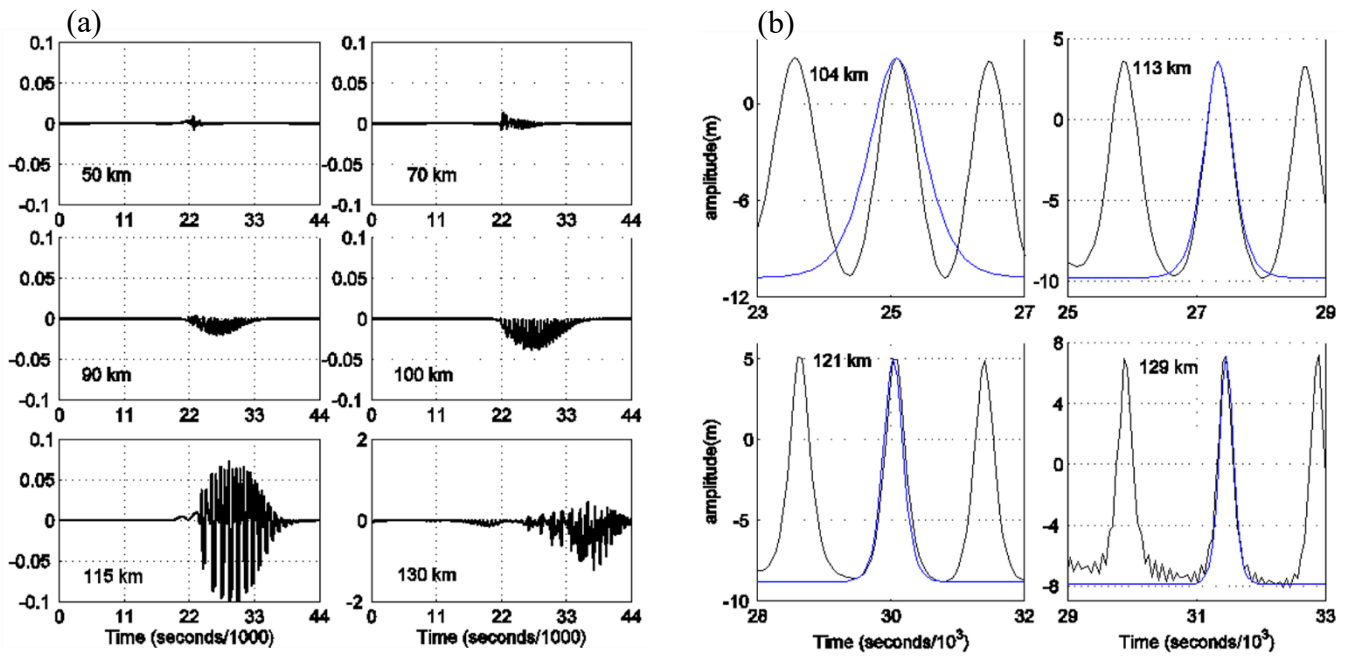


Fig. 2. Case A, (a) difference between the magnitudes of the nonlinear and dispersive terms at various distances from the boundary, and (b) leading waves of elevation (black line) at various distances $l > 100\text{km}$ from the boundary plotted with individual sech^2 waves (blue lines) within KdV model framework.

5

10

15

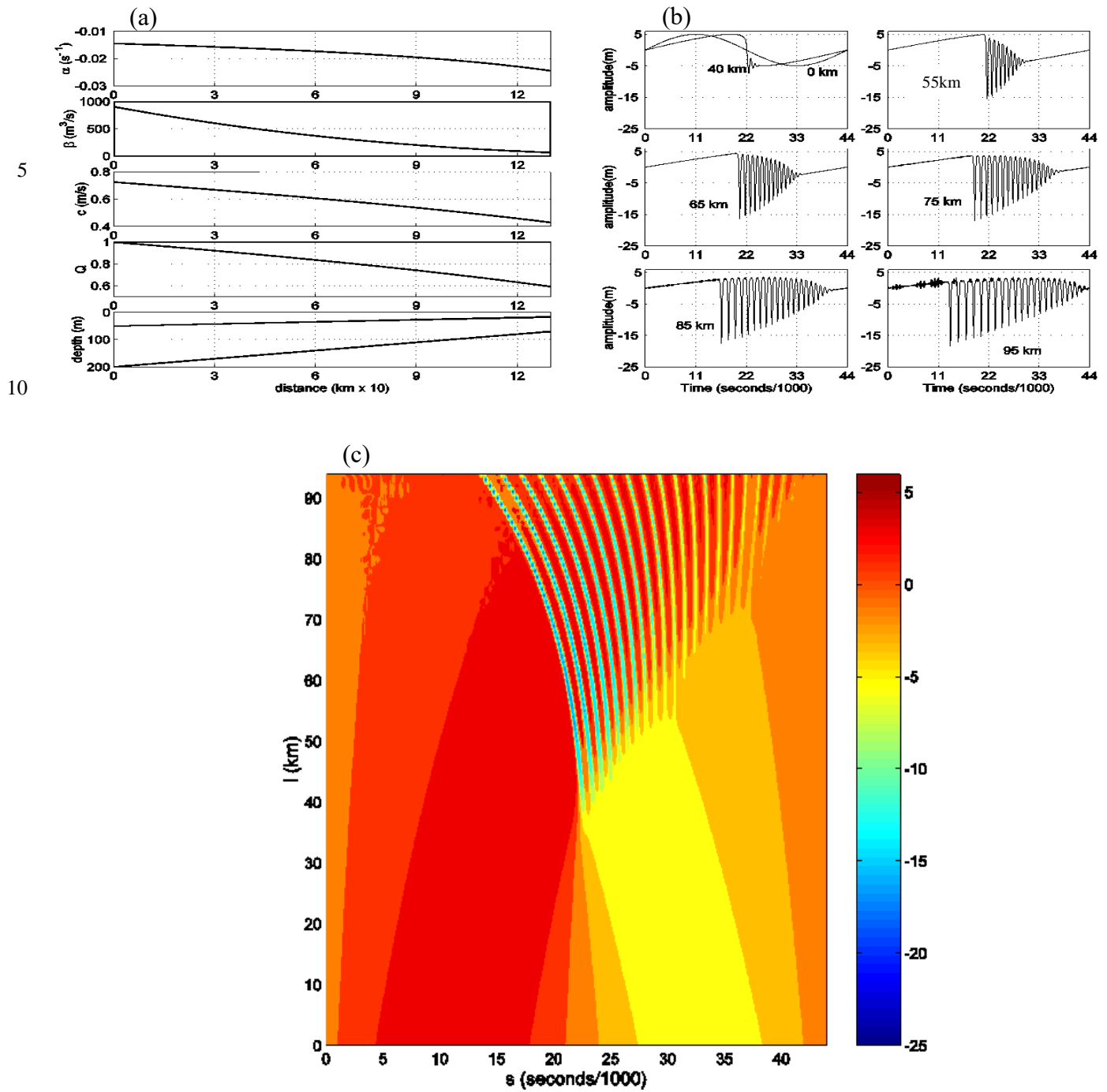


Fig. 3. Same as Fig. 1 but for Case B (constant sloping bottom with sloping interface).

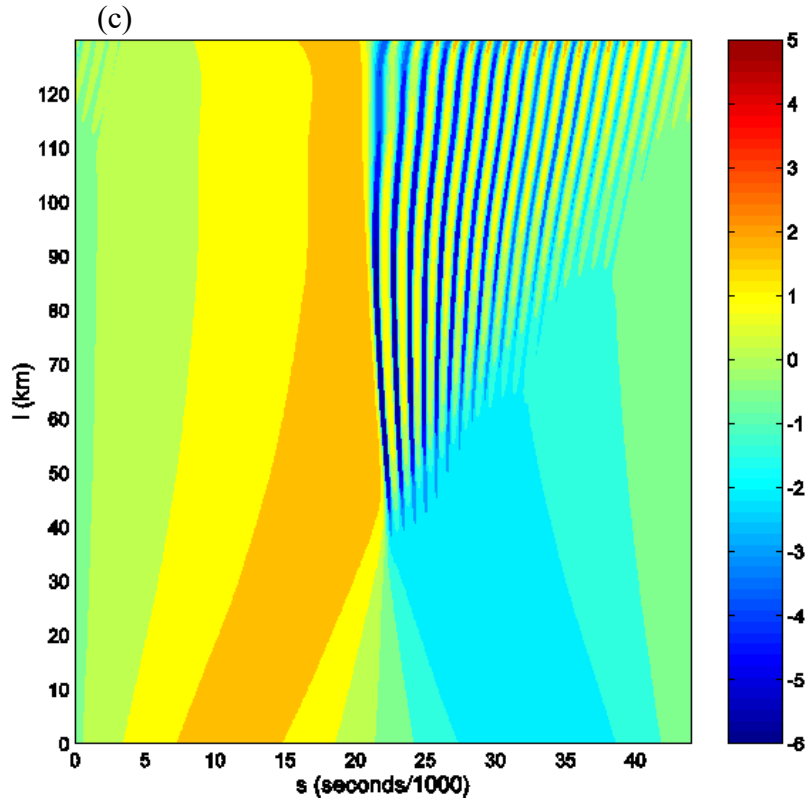
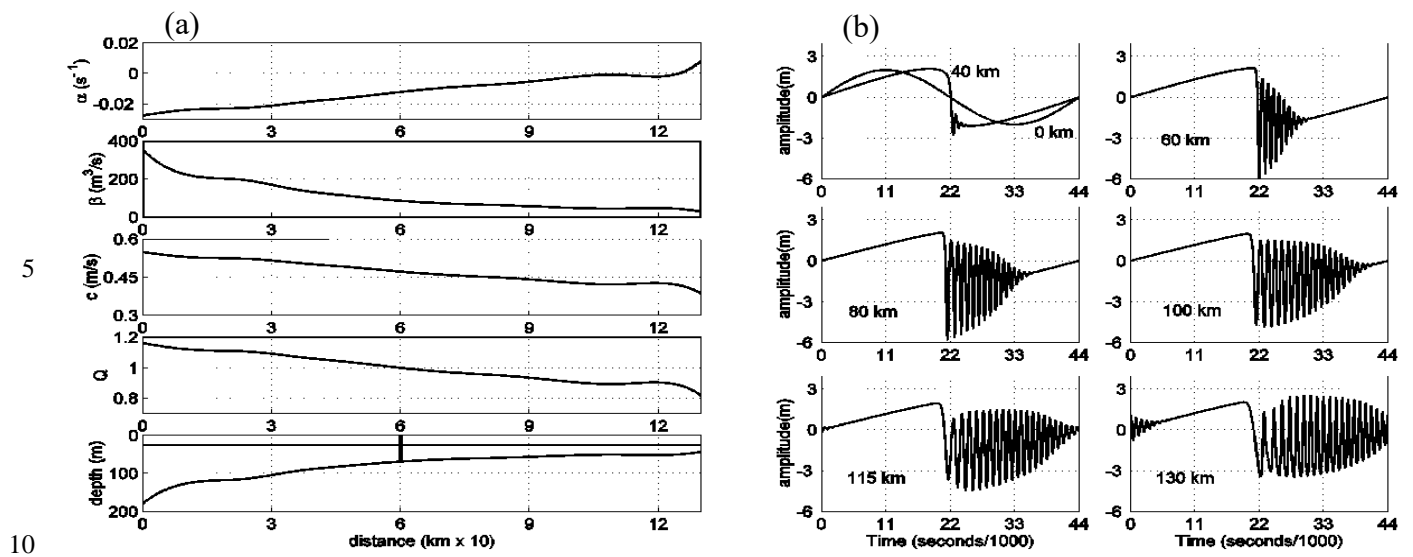


Fig. 4. Same as Fig. 1 but for CMO experiment site (with flat interface, $h_1 = 25$ m).

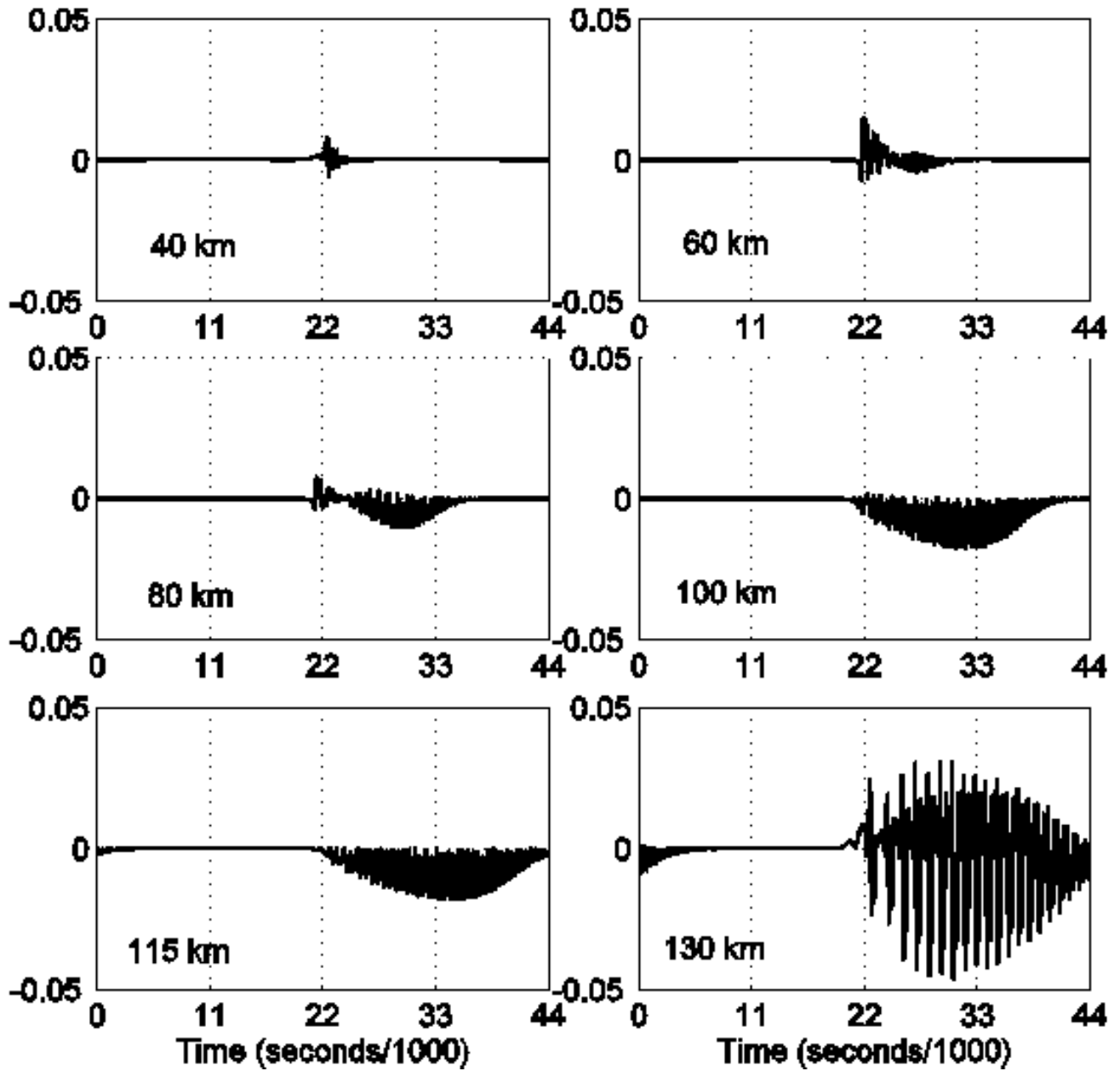


Fig. 5. CMO experiment site (with flat interface, $h_1 = 25 \text{ m}$) difference between the magnitudes of the nonlinear and dispersive terms at various distances from the boundary within KdV model framework.

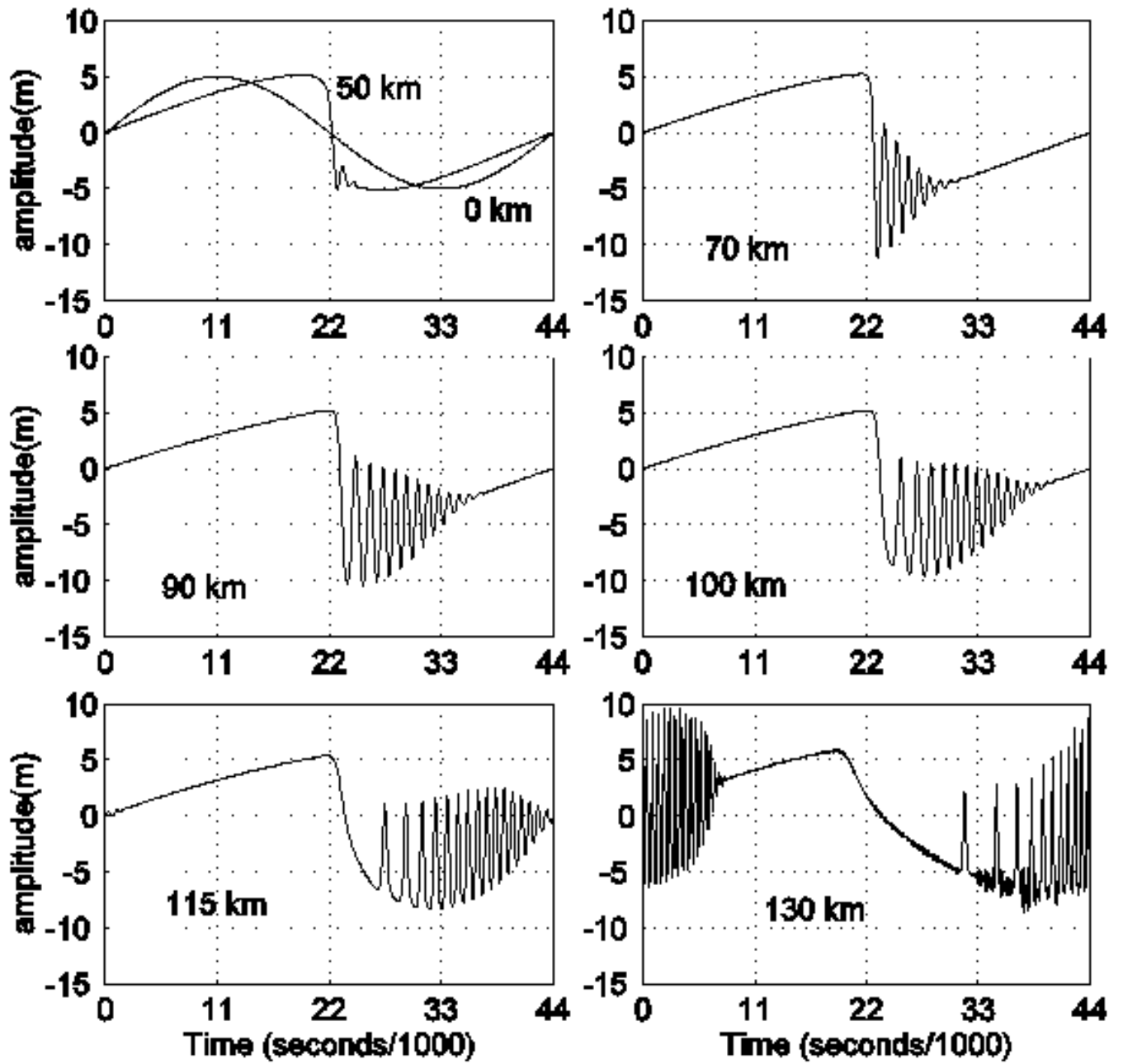


Fig. 6. Case A (constant sloping bottom with flat interface, $h_1 = 50 \text{ m}$) amplitude of the internal mode for two-layer fluid at various distances from the boundary within eKdV model framework.

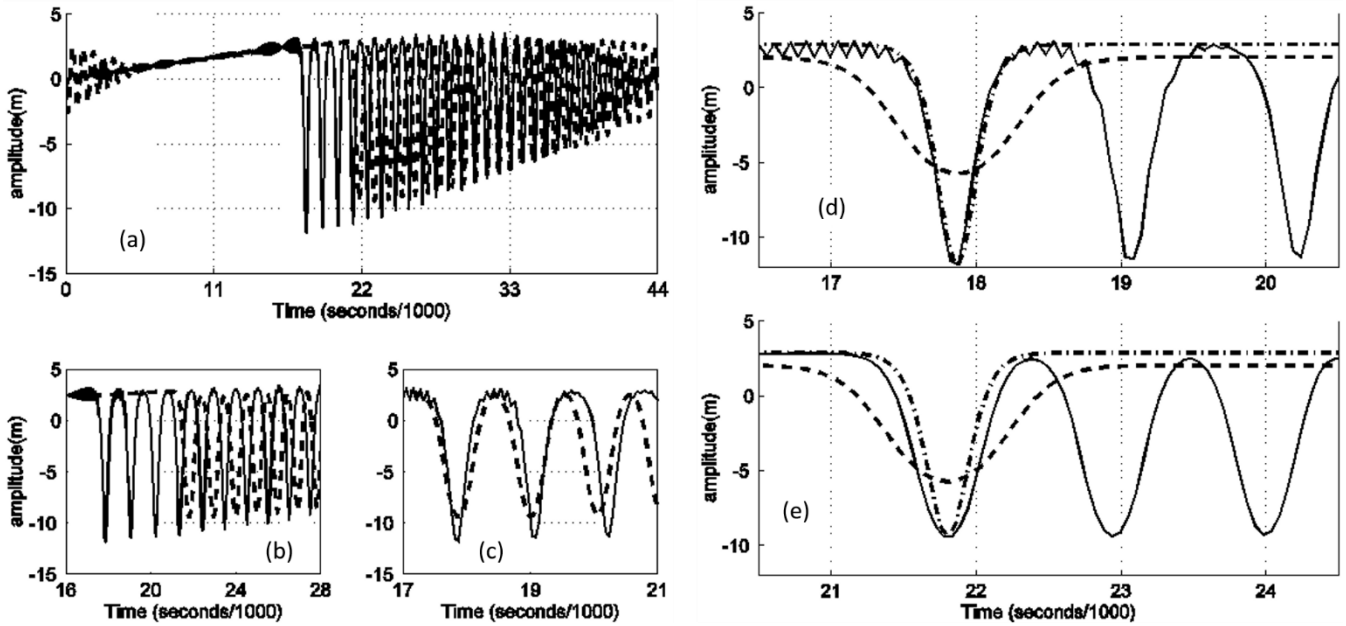
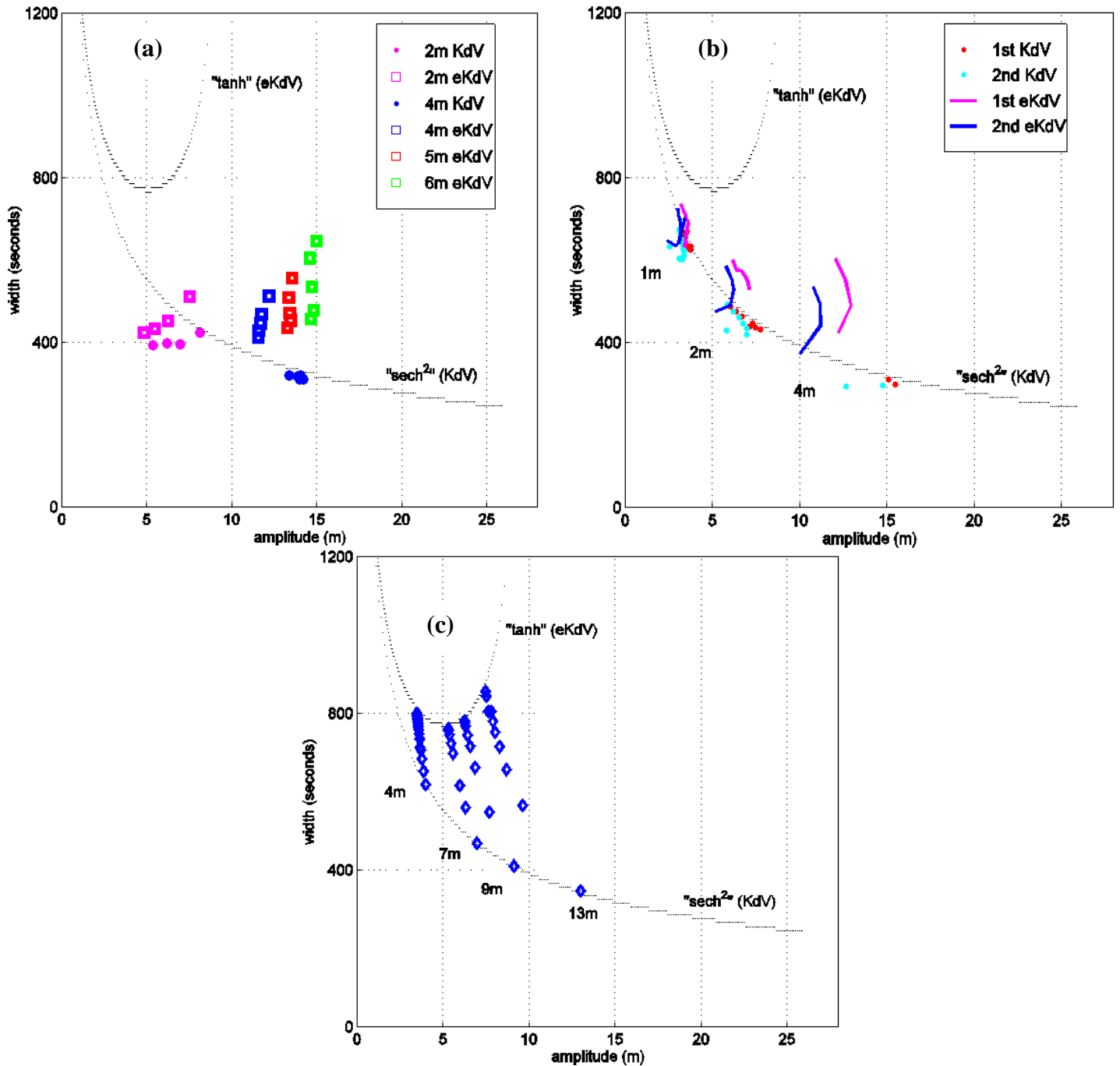


Fig. 7. CMO experiment site (realistic topography with level interface, $(h_1 = 25 \text{ m})$ amplitude of the internal mode for two-layer fluid at 60 km in 69 m depth water (CMO mooring site). **(a)** Comparison of KdV (solid line) and eKdV (broken line) solutions. **(b)** Close up of (a). **(c)** Leading KdV model waves (solid line) with superimposed eKdV model waves (broken line) shifted forward in time (s) so that the leading waves coincide. **(d)** and **(e)**. The leading wave of depression (solid line) plotted with an individual sech^2 wave (dot-dash line) and with an individual tanh wave (dashed line) for KdV model (d), and eKdV model (e).

10

15



15 Fig. 8 Width vs. amplitude of the leading waves of the KdV and eKdV solutions at the CMO mooring site ($h_1 = 25\text{ m}, h_2 = 44\text{ m}$) at 60 km from the boundary in 69 m depth water. Results for initial tidal amplitudes of 2, 4, 5, and 6 m are shown. The theoretical values for sech^2 and tanh waves using local

parameters are also shown (dotted lines). The width is calculated at 42% of the total amplitude. **(b)** Evolution of the width vs. amplitude of the two leading waves of the KdV and eKdV solutions for flat bottom ($h_1 = 25$ m, $h_2 = 44$ m) with same parameters as at the CMO site. Results for initial tidal amplitudes of 1, 2, and 4 m are shown. A value is plotted every 10 km for the 1 m tide beginning at 160 km and the lines run from 160 km to 260 km. A value is plotted every 20 km for the 2 m tide beginning at 80 km and the lines run from 80 km to 200 km. A value is plotted every 20 km for the 4 m tide beginning at 40 km and the lines run from 40 km to 100 km. The theoretical width vs. amplitude for sech^2 and tanh waves is also shown (dotted lines), and the width is calculated at 42% of the total amplitude. **(c)** Evolution of the width vs. amplitude of four solitary sech^2 waves of the eKdV solutions for flat bottom ($h_1 = 25$ m, $h_2 = 44$ m) with same parameters as at the CMO site. Results are shown for sech^2 amplitudes of 4, 7, 9 and 13 m. A value is plotted every 1 km up to a maximum distance of 15 km. The theoretical width vs. amplitude for sech^2 and tanh waves is also shown (dotted lines). The width is calculated at 42% of the total amplitude.

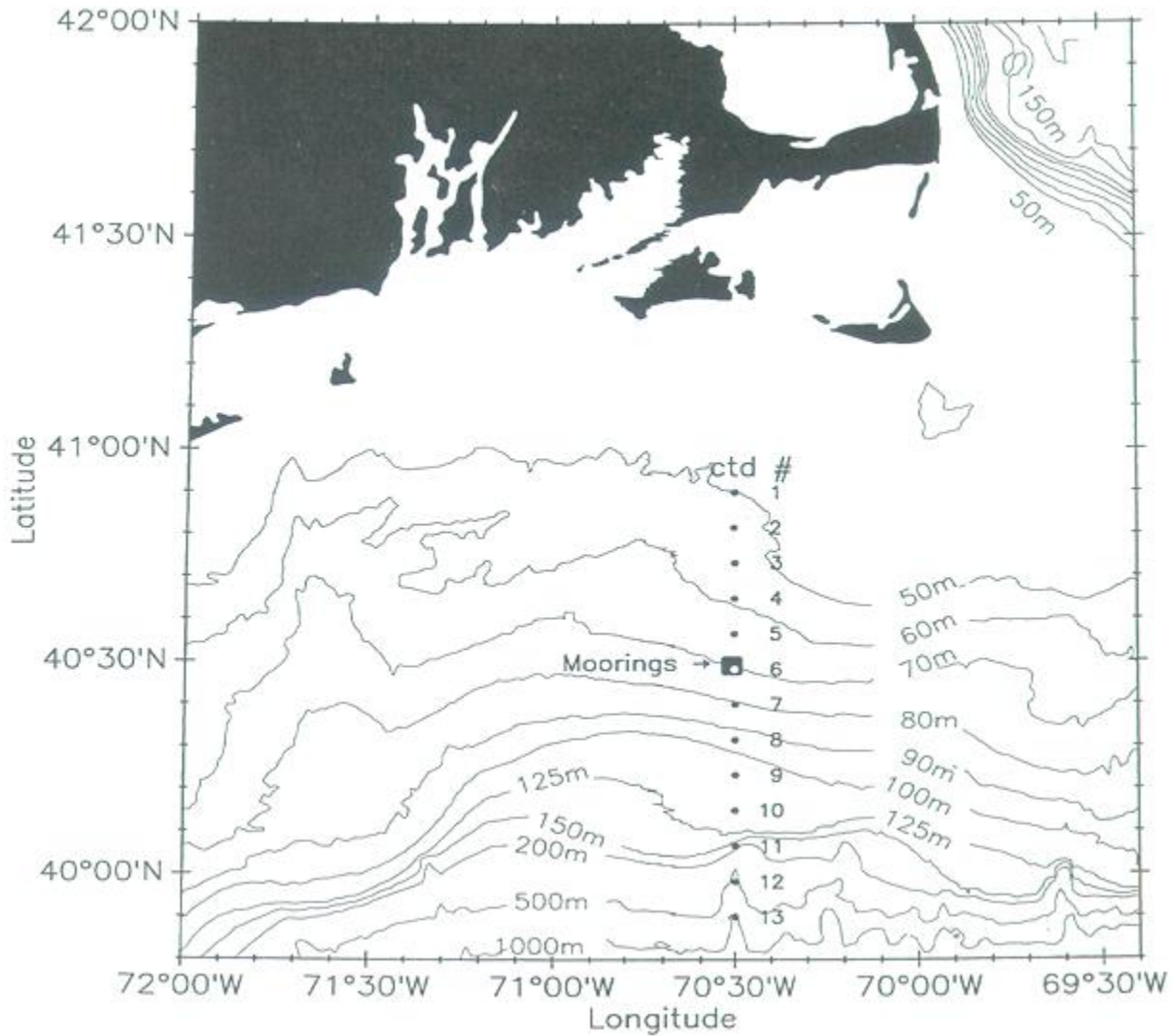


Fig. 9. Site of the Coastal Mixing & Optics experiment (left) located in the Middle Atlantic Bight to the south of Massachusetts. The data discussed was collected at the mooring marked 'CTD #6'.

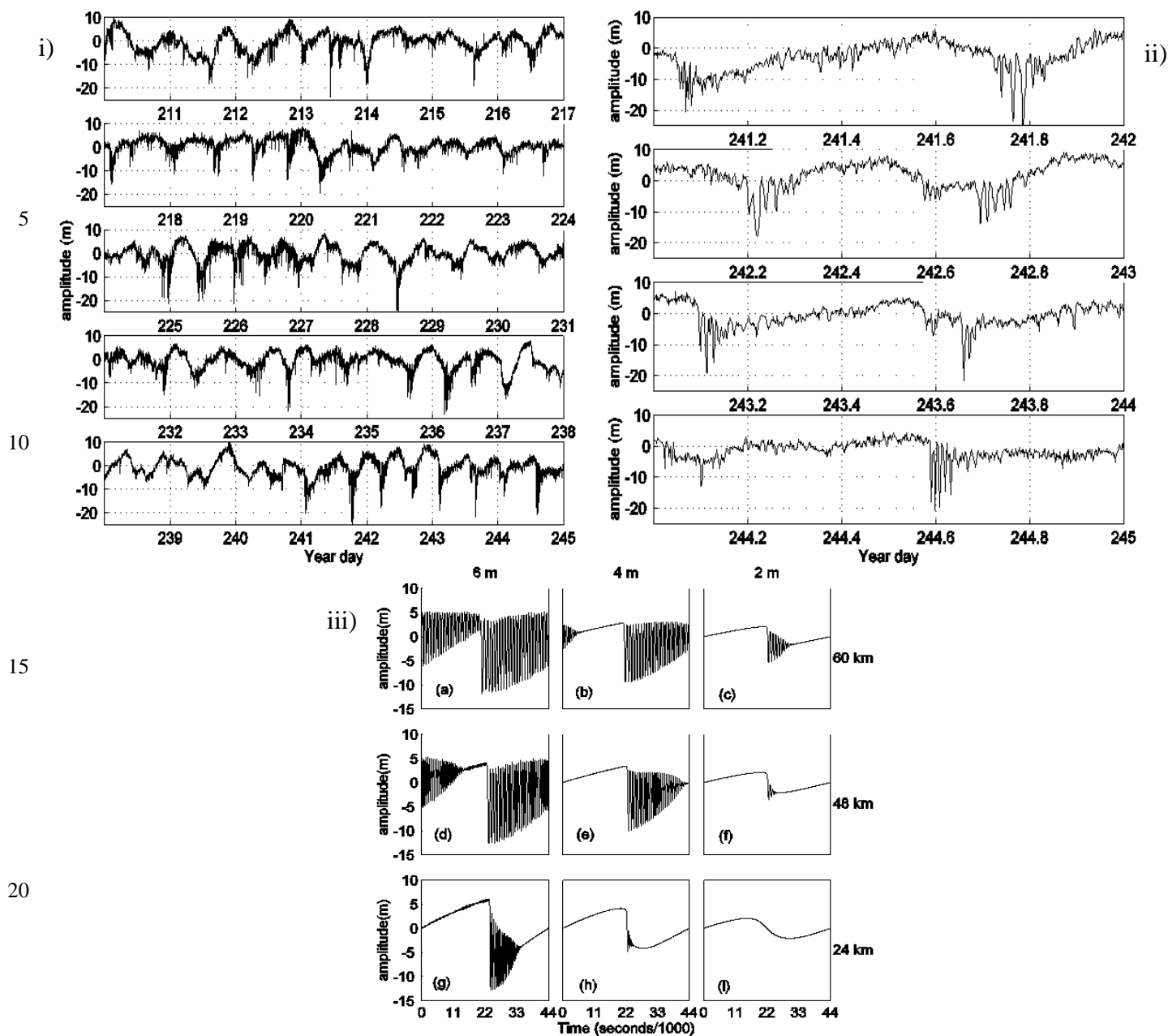


Fig. 10. Top left, i), amplitude of the first internal mode calculated from the current meter record at the CMO mooring site over the period day 210-245 of 1996. Top right, ii), Same as i) except for the period day 241-245. Bottom, iii), three sinusoids of amplitude 2 m, 4 m and 6 m, respectively, and with tidal period, as they appear at the CMO mooring site in the eKdV framework. The sinusoids have propagated shoreward from boundaries at 60 km, 48 km and 24 km offshore, respectively.

PRIMER Low Pass Filtered Pressure (db)

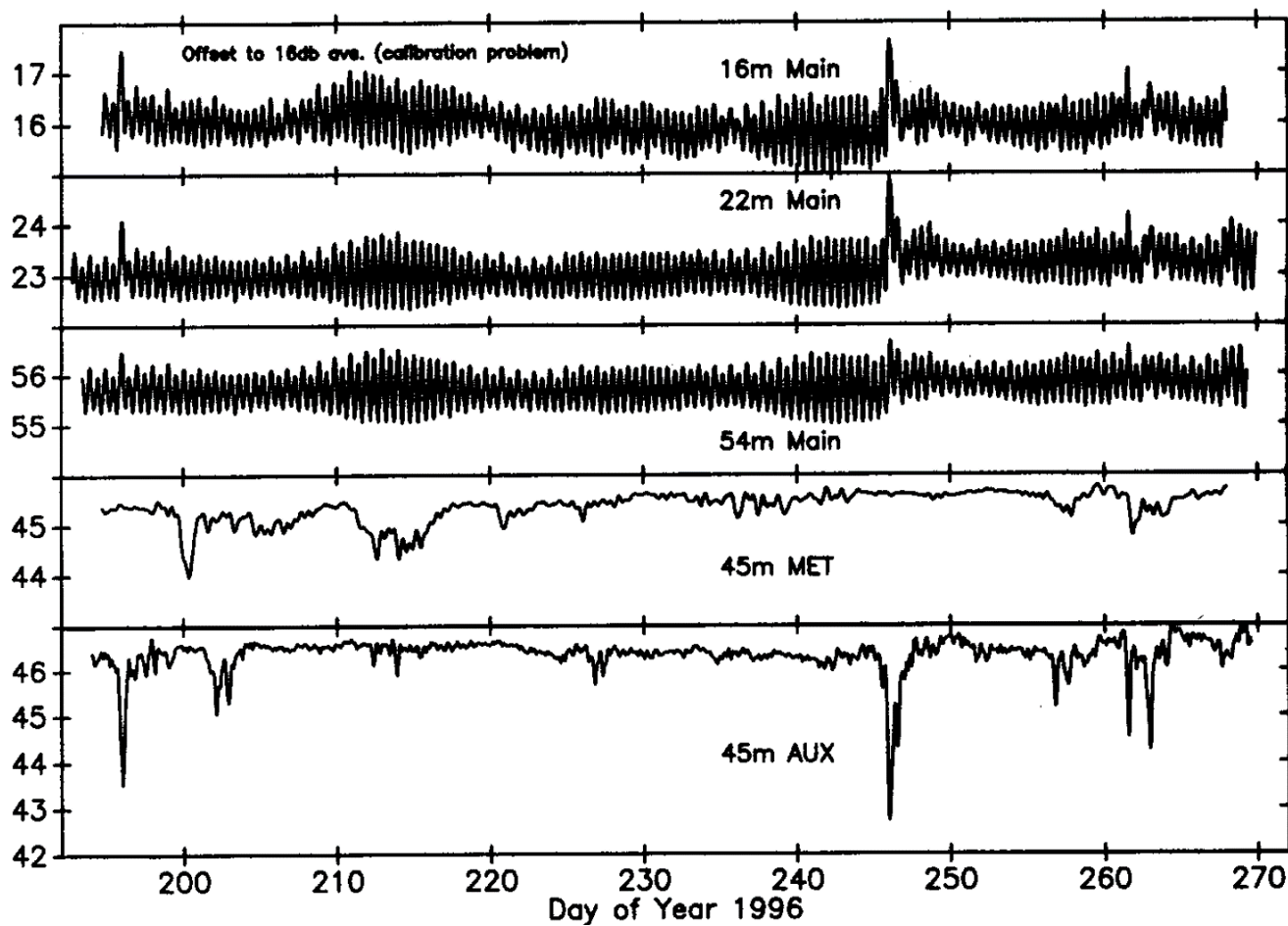


Fig. 11. Pressure (tidal) record at the CMO mooring site including for the period day 210 – 245 1996 (from Boyd et al., 1997).

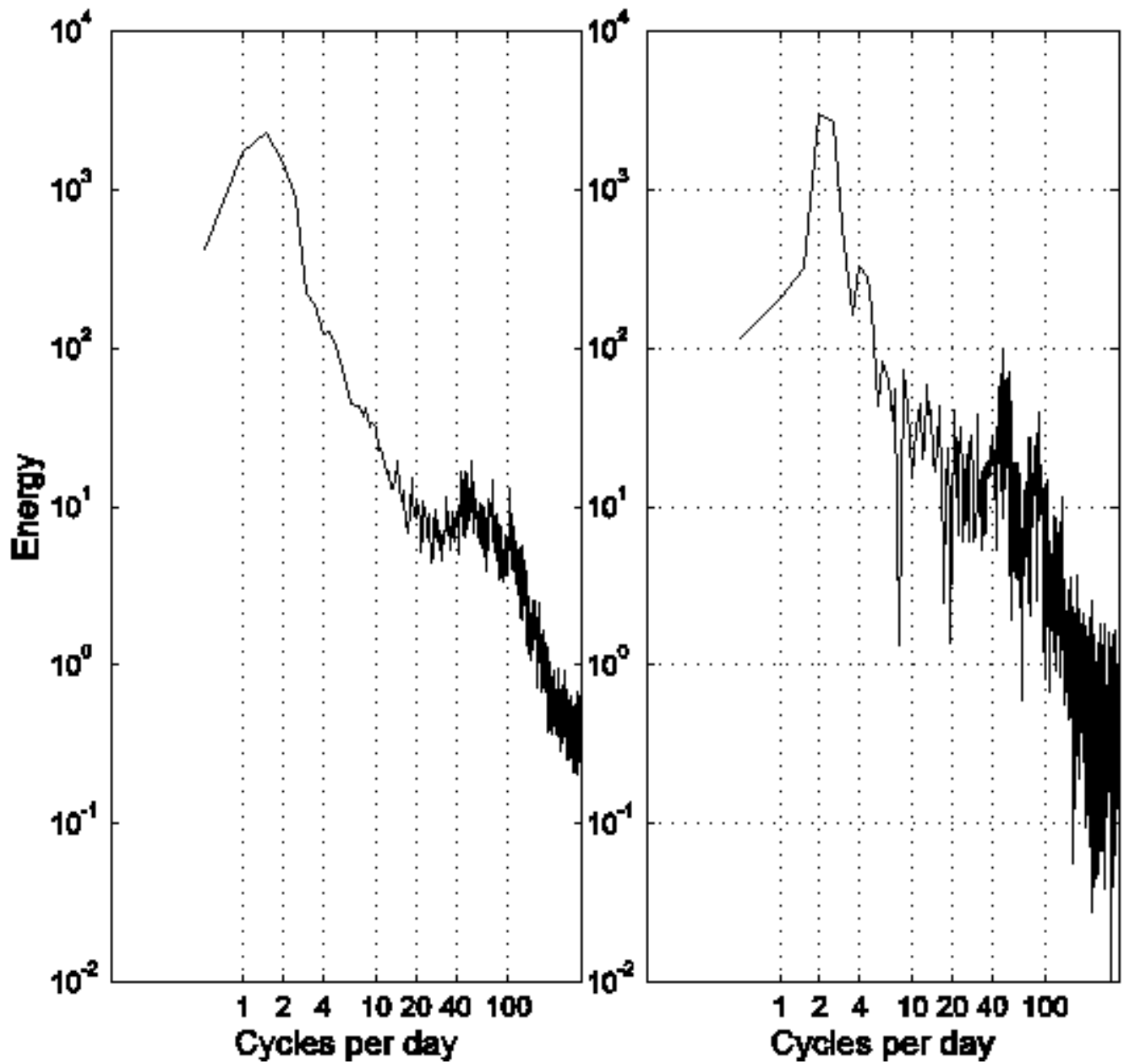


Fig. 12. Energy spectra of the first internal mode at the CMO mooring for the period day 210 – 245 (left), and the period 241 – 245 (right).

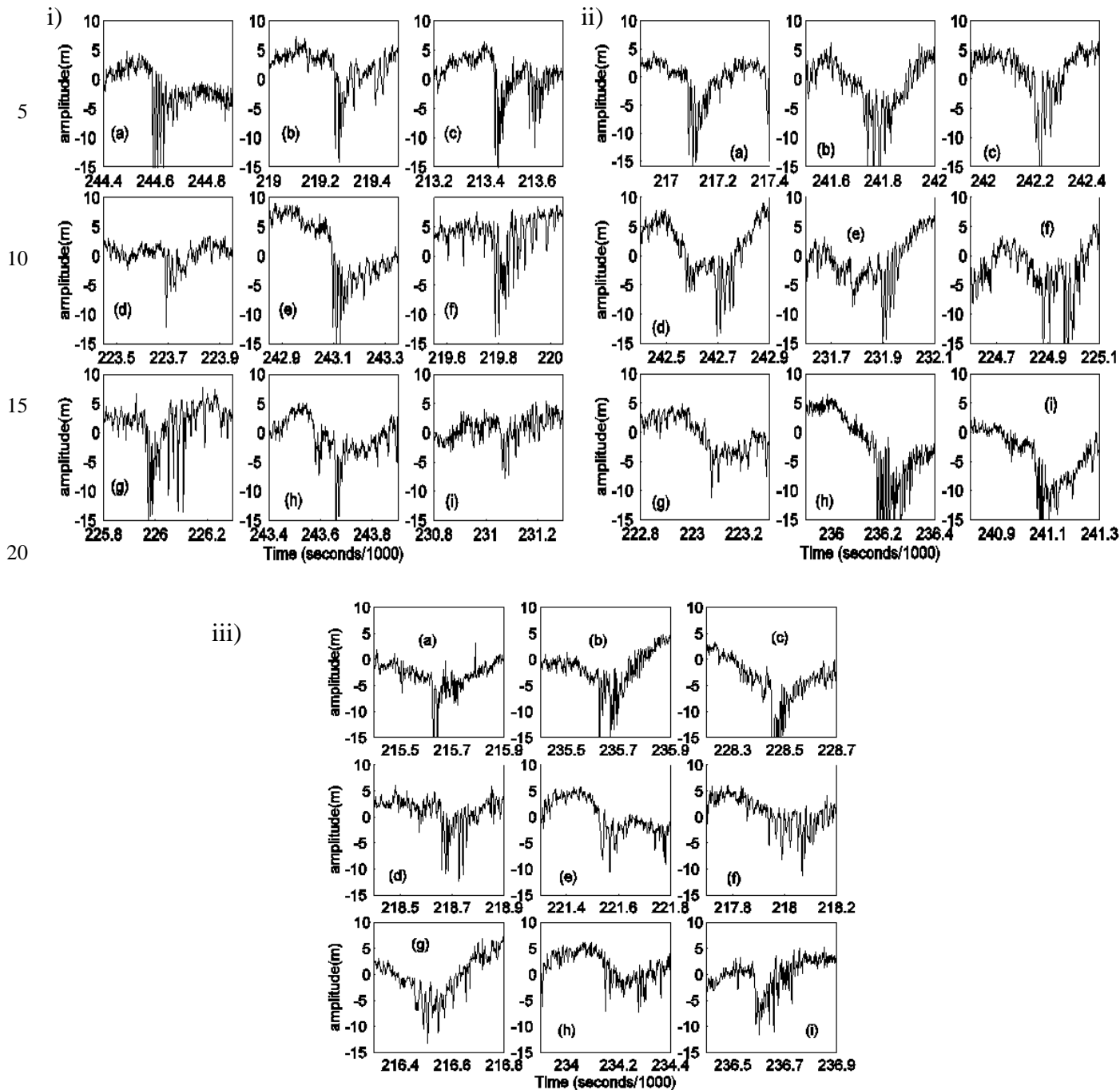


Fig. 13. Observations at the CMO Mooring site over a semi-diurnal period. Top left, i), sections of the record similar to events observed over a tidal period in the model runs of Fig. 10 iii). Top right, ii), same as i) except the record is a little bit more complicated over a tidal period. Bottom, iii), same as ii).

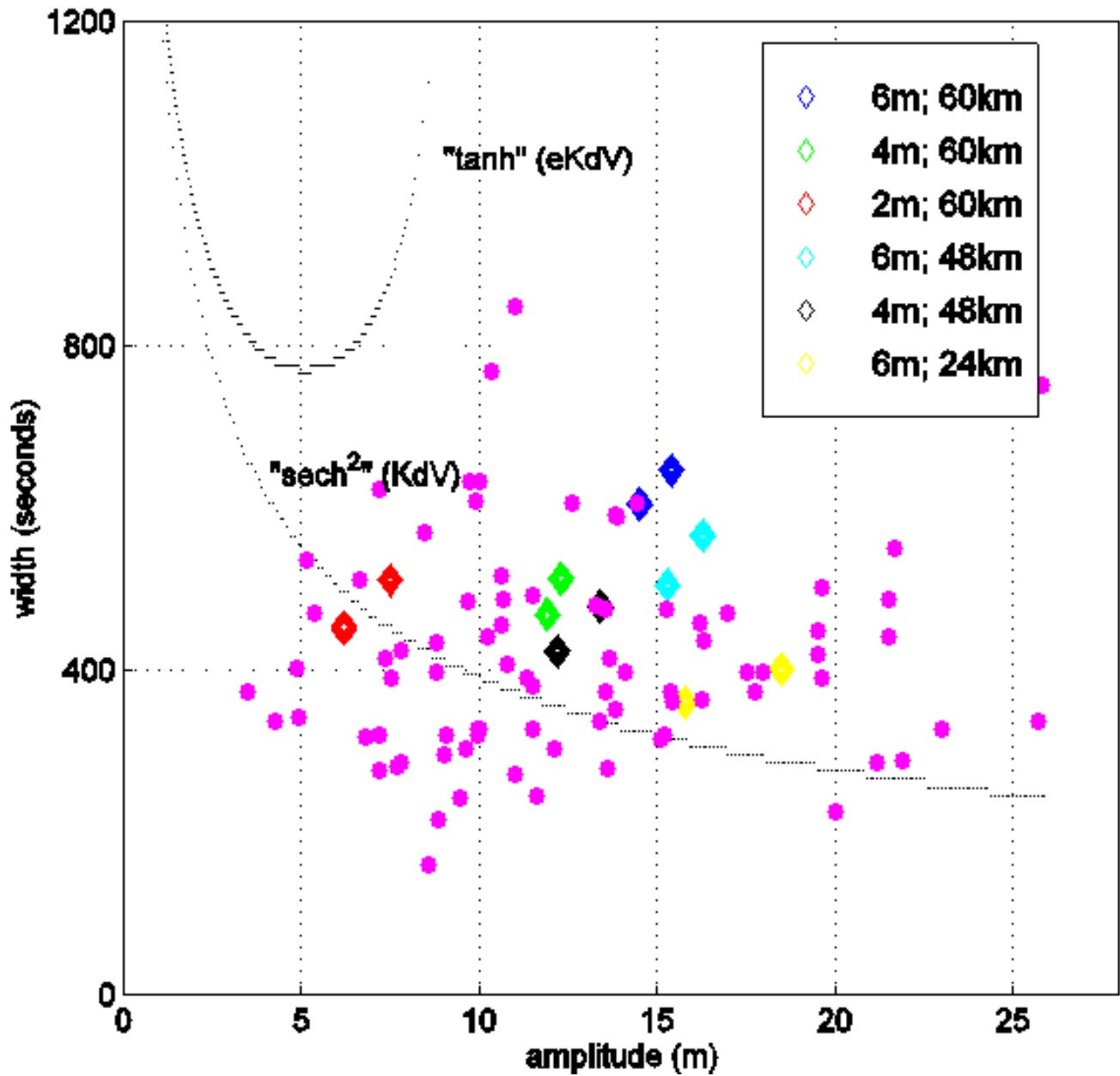


Fig. 14. Wave amplitude vs. wave width at the CMO mooring for waves from all events during the period day 210 - 245. Also plotted are the two leading waves from six of the nine model runs shown in Fig. 10 (diamonds).

Supplementary Figure

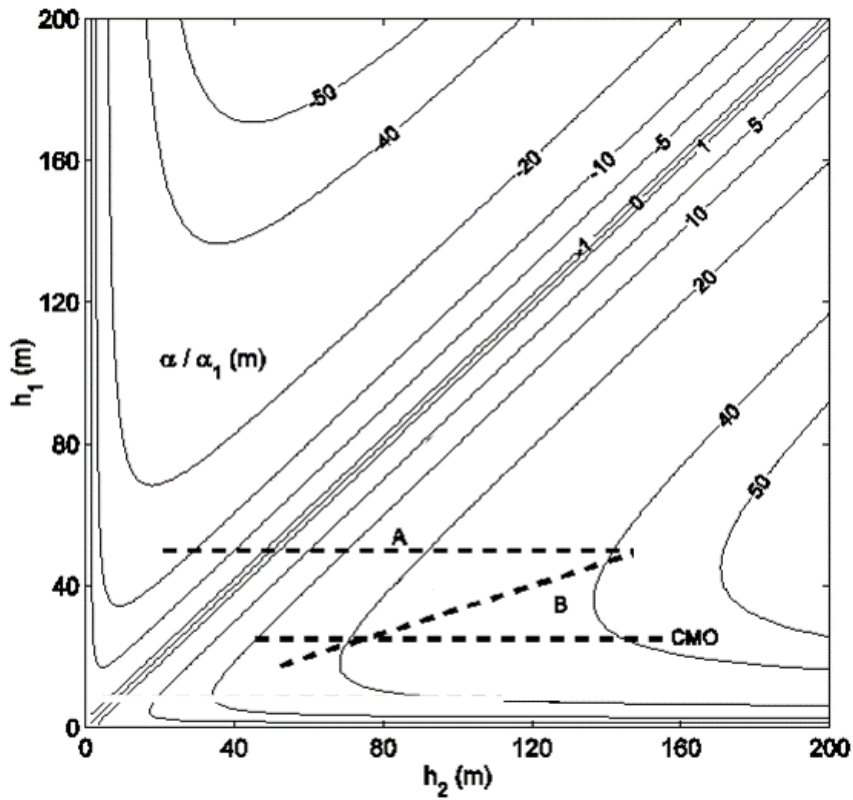


Fig. S1. Quadratic nonlinear parameter, α , divided by the cubic nonlinear parameter, α_1 , as a function of the depth of the upper layer, h_1 , and lower layer, h_2 . Values for sloping bottom (Cases A and B) and realistic slope and stratification at the CMO site are shown by the broken lines.